Available online at www.sciencedirect.com
SCIENCE DIRECT
Remote Sensing of Environment 100 (2006) 265 – 279
Remote Sensing of Environment
www.elsevier.com/locate/rse

Green leaf phenology at Landsat resolution: Scaling from the field to the satellite

Jeremy Isaac Fisher *, John F. Mustard, Matthew A. Vadeboncoeur

Geological Sciences, Brown University, Box 1846, 02904 Providence, RI, United States

Received 25 July 2005; received in revised form 19 October 2005; accepted 20 October 2005

Abstract

Despite the large number of in situ, plot-level phenological measurements and satellite-derived phenological studies, there has been little success to date in merging these records temporally or spatially. In this research, we bridge this scale gap through higher resolution satellite records (Landsat) and quantify the accuracy of satellite-derived metrics with direct field measurements. We compiled fifty-seven Landsat scenes from southern New England (P12 R51) from 1984 to 2002. Green vegetation areal abundance for each scene was derived from spectral mixture analysis and a single set of endmembers. The leaf area signal was fit with a logistic-growth simulating sigmoid curve to derive phenological markers (half-maximum leaf-onset and offset). Spring leaf-onset dates in homogenous stands of deciduous forests displayed significant and persistent local variability. The local variability was validated with multiple springtime ground observations (r^2=0.91). The highest degree of verified small-scale variation occurred where contiguous forests displayed leaf-onset gradients of 10–14 days over short distances (<500 m). These dramatic gradients occur in of low-relief (<40 m) upland regions. The patterns suggest that microclimates resulting from springtime cold-air drainage may be influential in governing the start of leaf growth; every 4.16 m loss in elevation delayed spring leaf onset by 1 day. These microclimates may be of crucial importance in interpreting in situ records and interpolating phenology from satellite data. Regional patterns from the Landsat analyses suggest topographic, coastal, and land-use controls on phenology. Our results indicate that deciduous forests in the Providence, RI metropolitan area leaf out 5–7 days earlier than comparable rural areas. The platform-independent curve-fit methodology may be extended across platforms and field data. The methodologically consistent approach, in tandem with Landsat data, allows an effective scaling from plot to satellite phenological observations.

Keywords: Green leaf phenology; Landsat vegetation and climate dynamics; Deciduous forest; New England; Microclimate; Urban heat island

1. Introduction

Green leaf phenology is the temporal pattern of seasonal leaf development and senescence as determined by climate, day-length, species type, age, and substrate (Schaber & Badeck, 2003; Wolfe et al., 2005). The timing of leaf development in many temperate deciduous species correlates with cumulative springtime temperatures (Cannell & Smith, 1983; Lechowicz, 1984; Rötzer, Grote, & Pretzsch, 2004). Recent modeling indicates that net carbon flux in temperate deciduous forests may be strongly influenced by the length of the growing season (White, Running, & Thornton, 1999) and interannual temperature variability (Cao & Woodward, 1998; Hollinger et al., 2005). An accurate understanding of phenology is thus important in large-scale biosphere models (Aber et al., 1995; Myneni et al., 1997; Potter et al., 2003; Running & Nemani, 1991). The coarse-scale remotely sensed inputs into these models depend on verification from field-based studies, a task which has had largely mixed results. We propose that local scales of variability alter existing interpretations of coarse-resolution remote sensing phenology and lend insight into observed patterns and drivers of deciduous phenology.

The study of phenology is currently guided by two independent research modes: (1) long-term plot and plant observations to reconstruct recent climatological trends in specific locations (e.g. Arora & Boer, 2005; Chuine, Cambon, & Comtois, 2000; Hunter & Lechowicz, 1992; Lechowicz, 1984; Schaber & Badeck, 2003), and (2) the exploration of spatial and temporal patterns through the use of high-temporal, but coarse-spatial resolution satellites (e.g. Duchemin, Goubier, & Courrier, 1999; Jenkins et al., 2002;

* Corresponding author. Tel.: +1 401 863 9845; fax: +1 401 863 2058.
E-mail address: Jeremy_Fisher@brown.edu (J.I. Fisher).

0034-4257/$ - see front matter © 2005 Elsevier Inc. All rights reserved.
doi:10.1016/j.rse.2005.10.022

Moulin et al., 1997; Reed et al., 1994; Schwartz, Reed, & White, 2002; White, Thornton, & Running, 1997; Zhang et al., 2004a). Long-term plot-based studies are essential in building an understanding of drivers and trends of phenology. Remote sensing phenology research expands the applicability of point-studies to broader spatial scales (e.g. Pellikka, 2001; White et al., 1997; Zhang et al., 2003) and critically tests empirical phenology models (e.g. Jenkins et al., 2002; Schwartz & Reed, 1999; White et al., 2002).

To date, there has been little success in tying together field and satellite-based research modes due to two significant challenges: field-to-satellite scaling and comparable phenological metrics. Field-to-satellite scaling is difficult due to the large spatial step required to bridge point studies and coarse resolution satellites; in broad-scale studies, compositional errors and the loss of high frequency data are frequent (Rastetter et al., 1992). Culling comparable phenological data from satellite data and field information is also problematic: few satellite phenology studies use metrics with validated physical meaning, and field data may not represent information which can be interpreted in satellite data. A limited number of studies have parameterized the relationship between ground-observed phenological stage and remotely sensed deciduous canopy development (Asner, 1998; Pellikka, 2001; Song, Woodcock, & Li, 2002). Although broad spatial patterns from remote sensing phenology indicate qualitative similarity to ground observations (Jenkins et al., 2002; Schwartz & Reed, 1999; White et al., 1997), there are still significant limitations to using these two data sources in tandem, as described above. In this paper, we describe a mechanism which successfully scales phenology metrics from ground observations to a high resolution remote sensing platform and provides a critical step between field and coarse-scale phenology studies.

Remote sensing phenological models have been produced at coarse scales, ranging from kilometers (using the Moderate Resolution Imaging Spectrometer-MODIS, Zhang et al., 2003, and the Advanced Very High Resolution Radiometer-AVHRR, Duchemin et al., 1999) to degrees (AVHRR: Jenkins et al., 2002; Moulin et al., 1997; Reed et al., 1994; White et al., 1997). Landsat Thematic Mapper data at 30 m resolution has been utilized to classify the phenological behavior of agricultural crops over the course of a season (Badhwar, 1984) and estimate productivity in forest stands (Goetz & Prince, 1996). In this research we utilize an 18-year record (1984–2002) of Landsat TM and ETM+ data to model eastern deciduous forest (EDF) phenologies in southern New England. At Landsat resolution, we are able to explore patterns within and among stands of pure EDF and assess model predictions in the field.

Based on previous phenological work, we may expect a high degree of local variability due to species composition (Chuine et al., 2000; Hunter & Lechowicz, 1992; Lechowicz, 1984; Schaber & Badeck, 2003), forest structure (Seiwa, 1999), topographic variation (Pellikka, 2001; Morecroft, Taylor, & Oliver, 1998), substrate (Côté et al., 1998), and the influence of anthropogenic changes in the forest canopy (including selective cutting or the introduction or planting of non-native tree species) and understory (such as the planting of grass or horticultural species). Indeed, we observe a high degree of phenology variance at the 30-m pixel scale. Thus a more complete understanding of fine-scale spatial variability is critical when assessing coarse-scale phenological results.

1.1. Identifying phenologically important dates

EDF is phenologically uni-modal, exhibiting a clearly defined period of budburst and leaf growth (greenup), followed by senescence and leaf abscission. From an optical remote sensing perspective, this cycle appears as increasing then decreasing canopy greenness. However, the periods of early leaf growth and chlorophyll accumulation, as well as leaf senescence and abscission often extend over several weeks (Parker & Tibbs, 2004). Seasonal phenological markers (the beginning and end of the growing season) are typically reported as occurring on a particular day-of-year (DOY). The method in which DOY phenological markers are identified is a non-trivial pursuit.

There are multiple approaches and modifications for finding phenological markers from multi-temporal satellite data. These approaches range from simple smoothing to non-linear inverse modeling approaches. Most phenological detection algorithms utilize the normalized difference vegetation index (NDVI) from AVHRR or Enhanced Vegetation Index (EVI) and NDVI data from MODIS, and most utilize Maximum Value Composite (MVC) data. The MVC filter (Holben, 1986) is designed to find the highest NDVI (and therefore lowest noise) in a within fixed time increment. However, MVC introduces temporal uncertainty when the acquisition DOY falls within a week- to month-long window, but is commonly time-stamped as the window center DOY. Such uncertainty renders MVC data potentially inappropriate for tracking 1–2 week phenological events or interannual variability which is often less than 1 week.

The least computationally intense approaches for finding satellite-based phenologies assume an accurate and complete temporal greenness profiles. Moulin et al. (1997) and Ebata and Tateishi (2001) take the first derivative of non-smoothed and smoothed composite NDVI time series (respectively) to find the inflection point DOYs, a method which is extremely responsive to the addition of noise in sparse time series. Reed et al. (1994) compares raw composite time series to smoothed version of the same time series (using a 126-day moving average) to find "crossover" DOY points (where the smoothed and unsmoothed time series cross each other), which yields phenological markers with uncertain physical meaning. Schwartz et al. (2002) and White et al. (2002) fit composite time series with point-to-point splines (which pass through every data point), and in doing so assume that all NDVI data in the series are both exact and temporally accurate; phenological markers are found where the NDVI composite series reaches the average between the maximum and minimum NDVI values ($NDVI_{max}$ and $NDVI_{min}$, respectively), thereby assigning significant weight to $NDVI_{max}$ and $NDVI_{min}$ (any error in either will change the timing of the phenological markers). In this research, we use a low order-fit to the annual signal,

creating a robust solution but sacrificing high temporal frequency variations.

White et al. (1997) and Duchemin et al. (1999) utilize daily AVHRR NDVI data, eliminating the temporal uncertainty of composite datasets. Both researchers utilize the Best Index Slope Extraction (BISE) of Viovy and Arino (1992) to filter erroneous NDVI data and linearly fit the remaining data to find phenology markers. White et al. (1997) finds the half-maximum of the BISE-fit data (again assigning unjustified weight to $NDVI_{min}$ and $NDVI_{max}$), while Duchemin et al. (1999) fits a linear function to a time series subset to derive metrics. Jenkins et al. (2002) observes the date at which a composted AVHRR time-series crosses a threshold (NDVI=0.45); however, forests with high $NDVI_{min}$ (such as conifers) will appear to pass over the threshold quickly, while sparse canopy forests with a low $NDVI_{maz}$ may pass the threshold late or not at all. While the threshold system is used exclusively to find interannual variability, we may expect potential systematic error based on different forest structures and compositions.

More computationally intense methods for observing phenologies account for some of the described difficulties. The TIMESAT smoothing algorithm developed by Jönsson and Eklundh (2002) uses modified Gaussian curves to represent greenup and senescence, effectively utilizing the full suite of temporal greenness data. Badhwar (1984) and Goetz and Prince (1996) fit sparse greenness profiles with a complex six-parameter model. Zhang et al. (2003) pursues a similar method, using non-linear least-squares methods to fit composite MODIS EVI data with two sigmoid functions (one increasing with greenup, the other falling with senescence). A sigmoid fit method both utilizes all possible information and is robust to the addition of random noise. In this research, we modify and expand on the method proposed by Zhang et al. (2003) to incorporate a different data set (Landsat) with additional error and noise estimations.

1.2. The sigmoid structure of a phenology

In this research, we simplify the appearance of a growing canopy as a sigmoid logistic growth curve with horizontal asymptotes at time (t) $t_{-\infty}$ and t_{∞} (Zhang et al., 2003; Richardson et al., unpublished). A general sigmoid is given by the equation

$$y(t) = \frac{1}{1 + e^{m+nt}} \quad (1)$$

where $y(t)$ is the value at time t, and m,n are factors which control the phase shift and slope of the sigmoid structure. A sigmoid approximates a cumulative distribution function, such that it represents the accumulated sum of a probability density and the first derivative of $y(t)$ is nearly Gaussian. If we suppose that the probability for the DOY of the emergence of a single leaf is normally distributed, than the total amount of green cover through time is simply an accumulation, following a curve similar to that of logistic growth. Over a dense forest against a non-vegetated background, we could theoretically expect the area of green leaf cover to start at 0 (no leaf cover), and rise to 1 (complete leaf cover) as an accumulating function. In a coniferous forest, the curve may begin above 0, and if a pixel is mixed with non-vegetation, the maximum value may stay well below 1. Logistic growth in phenologies can be seen in data from ground observations of canopy closure (e.g. Kato & Komiyama, 2002; Pellikka, 2001; Richardson et al., unpublished), leaf development (e.g. Richardson et al., unpublished; White et al., 1997), salt marsh development (Bouzille, Bonis, Clément, & Godeau, 1997), maple stem growth (Côté et al., 1998), and leaf abscission (Dixon, 1976).

2. Methods

Vegetation areal abundance signals from spectrally unmixed Landsat scenes were fit with a two-part sigmoid curve representing greenup and senescence/leaf-abscission. We describe the field location, data source and preprocessing, the detection and down-weighting of noise, and finally, a solution for fitting temporally sparse, detailed Landsat data to produce a validated, field scale map of phenological variability.

2.1. Data extent

The satellite data encompasses the common area of 57 P12:R14 scenes collected from 1984–2002 from Landsat 5 TM and Landsat 7 ETM+. The data are temporally well distributed by DOY, and no year dominates either transition season (Fig. 1). The area covers Rhode Island (RI), eastern Connecticut (CT), and eastern Massachusetts (MA), including the cities of Boston, Providence, and Worcester, and is centered at 41.77°N, 71.36°W (see Fig. 5 inset). Southern New England is a densely populated region, with compact towns and cities interspersed through relatively broad tracts of EDF. Most of the EDF was converted to agricultural or working land in the 19th century; the vast majority of southern New England forests have regrown from old pastures, crop fields, and woodlots within the last century. Regional studies indicate that the forests are compositionally far more homogenous than might otherwise be expected from climate patterns (Foster, Motzkin, & Slater, 1998). The region has strong geological differentiation and climate gradients: southern and eastern moraine and outwash features rise into till-covered low-elevation rocky glacial topography inland; the interior experiences continental climates, while the climate of the south and east coasts are moderated by proximity to the Atlantic Ocean. The ocean temperatures in this area are warm in the fall and cool in the spring, lagging small water-bodies (and insolation) by approximately 1 month (Fisher & Mustard, 2004; Thomas, Byrne, & Weatherbee, 2002).

2.2. Data and preprocessing

All data were georeferenced to sub-pixel accuracy. Path radiance and atmospheric transmissivity differences between scenes were corrected to a scene collected on June 7, 1999

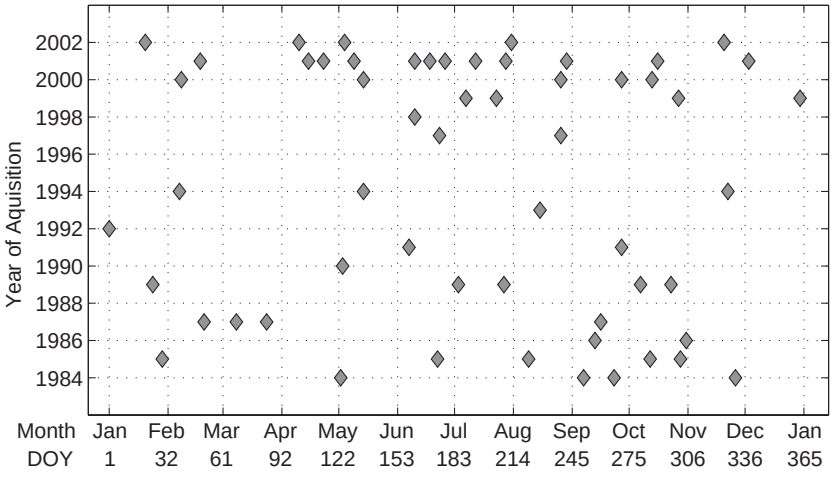

Fig. 1. Distribution of the 57 Landsat scenes utilized for this analysis.

(ETM+). The June 7th scene was corrected to units of reflectance by subtracting dark pixel values (to remove path radiance) and applying Landsat 7 standard corrections (NASA, 2003). Eighty (80) invariant points (large paved surfaces, sand and outcrops, and deep water) were collected in all scenes, and each scene was corrected to the June 7th scene using empirical line fits. Cloud and snow covered pixels were not included as invariant points.

Total vegetation abundance was derived from a spectral mixture analysis (SMA) of each of the 57 scenes. A SMA solution is preferable to NDVI or other indices as it does not saturate at high canopy coverage and has been shown to be linearly related to vegetation areal abundance (Elmore et al., 2000). Generalized endmembers (Small, 2004) were derived from two scenes (7/7/1999 and 10/13/2000) in an iterative process to find the best set of representative endmembers (Adams et al., 1993; Elmore et al., 2000; Mustard & Sunshine, 1999). The final selection included endmembers of green vegetation (GV), non-photosynthetic vegetation (senesced or dead vegetation), soil, and urban surfaces. Spectra were unmixed into fractions of endmembers using a least squares approach (no unit-sum or positive fraction constraint) and the root mean square error (RMSE) was generated for each data point by comparing predicted spectral profiles with observed Landsat spectra. Vegetation endmember fractional abundances (GV) were preserved and stacked by DOY to create a representative annual phenology (conceptually similar to Fisher and Mustard, 2004). By compressing 18 years of data into a single representative year, there is a necessary loss of interannual signal.

2.3. Seasonal phenology model

The sigmoid logistic growth model of a phenology effectively explains much of the temporal patterning observed in total canopy cover during a growing season. However, the difference between deciduous canopies, which reach nearly full leaf canopy cover, and coniferous forests, which maintain chlorophyll in the winter, is a scaling function which controls the average minimum and maximum greenness. Therefore, Eq. (1) is given a multiplicative amplitude parameter (v_{amp}) and additive minimum parameter (v_{min}).

Senescence and leaf abscission could be modeled as two separate multiplicative sigmoids of decreasing greenness (senescenc, Richardson et al., unpublished) and then loss of opacity (leaf-fall, Dixon, 1976) but here are simplified into a single negative logistic curve.

The full equation used to model green leaf phenology is

$$v(t) = v_{\min} + v_{\text{amp}}\left(\frac{1}{1+e^{m_1+m_2 t}} - \frac{1}{1+e^{m_3+m_4 t}}\right) \quad (2)$$

where $v(t)$ is the fraction of green cover (areal abundance) observed at DOY t, v_{min} and v_{amp} are the background greenness value and total amplitude, respectively. Parameters $m_{1,2}$ and $m_{3,4}$ are fitting parameters controlling phase and slope for both greenup ($m_{1,2}$) and senescence/abscission (m_3, m_4). Fig. 2 shows a schematic of the curve structure fit to the Landsat representative phenology at an example location. All model parameters are derived through non-linear inverse models applied independently to the GV time series of each pixel.

We define the date of leaf onset as the DOY at which the green cover reaches half maximum greenness. The half-maximum is the most stable and well constrained point in the curve. The half-maximum on the decreasing slope is the leaf offset, or loss of canopy structure. Onset and offset are calculated by finding the DOY at the maximum and minimum, respectively, of the first derivative of $v(t)$. Zhang et al. (2002) records 'greenup onset' and 'maturity onset' as the points of greatest curvature at the base and top of the sigmoid, respectively; we suggest that these metrics may be sensitive to early spring understory growth (Kato & Komiyama, 2002), thus changing the steepness of the curve, but not the curve midpoint. The date of leaf onset does not necessarily record the DOY of most vigorous growth; a forest with dense vertical structure may appear to reach half canopy coverage (date of leaf onset) more rapidly than a monolayer forest (Pellikka, 2001). Horizontal (areal) canopy coverage (stems per hectare) does not change the perceived onset date.

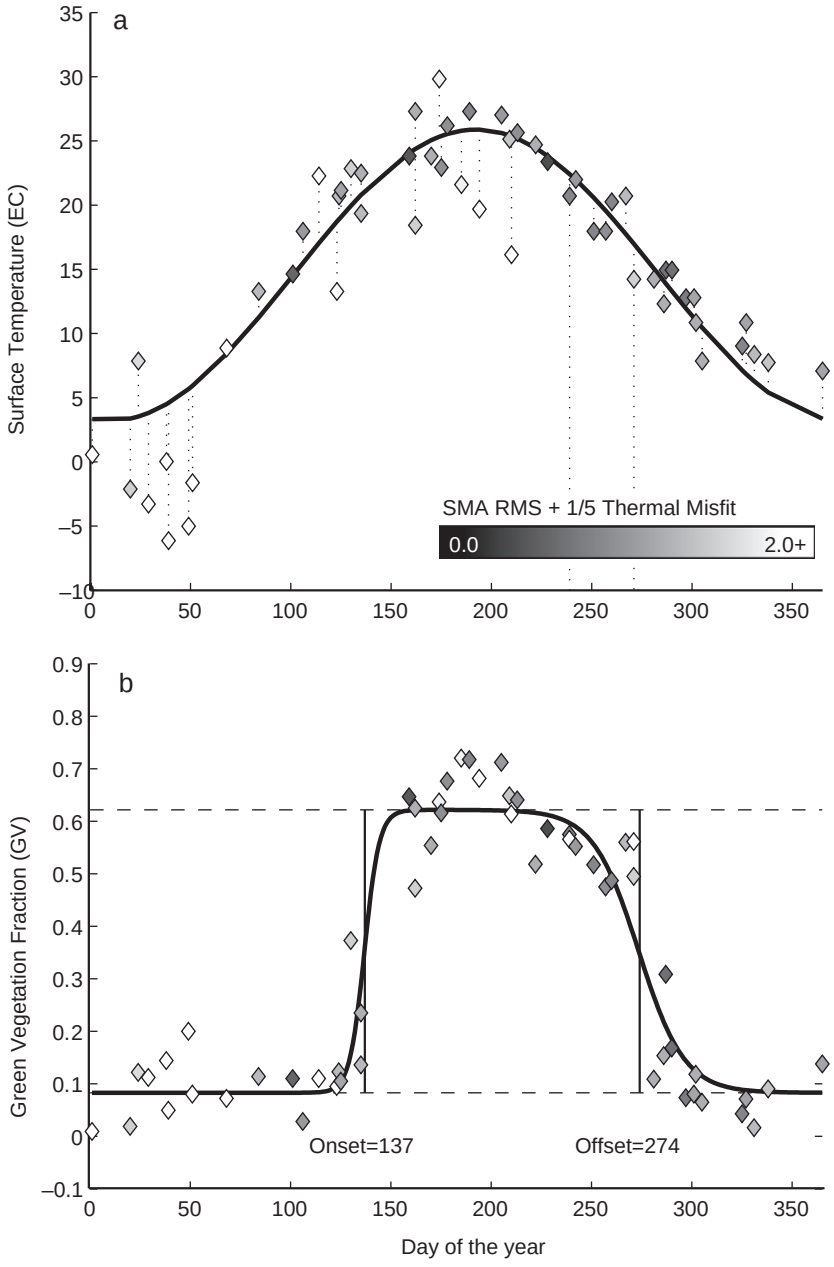

Fig. 2. Schematic of curve fitting mechanism. Land surface temperature (a) is derived from Landsat band 6 and fit with a maximizing envelope sinusoid. Data points which fall further from this line are subsequently assigned less weight in the phenological fit. Spectrally unmixed green vegetation fraction (b) is fit with a pair of logistic growth sigmoid functions. Points with the least temperature and spectral error are assigned a greater weight (darker colors in this schematic) in the curve fit. Finally, onset and offset are calculated as the half-maxima of the sigmoid curve.

The non-linear least squares model which we apply modifies the initial model parameter estimations of $m_{\text{first}} = [v_{\min} v_{\text{amp}} m_1 m_2 m_3 m_4]$ with iterative, incremental changes to the parameters. The set of parameters (m) are modified by incremental changes and perturbances (m_{pert}), which are calculated through a least squares inversion (see Menke, 1989 for a complete methodology):

$$m_{\text{pert}} = \left[G' W G + C_{\text{pp}}^{-1} \right]^{-1} G' W (d_{\text{res}}) \quad (3)$$

where G is a matrix of the partial derivatives of Eq. (2) with the estimate of the parameters (m) in the current iteration; d_{res} is the residual difference between the current estimate of the modeled curve $v(t)$ and the initial GV data GV(t); W is a diagonal weighting matrix which determines the importance of each individual data point in the final curve estimate. Weights are determined by the accuracy of each data point (discussed in the next section). Finally, C_{pp} is a 6×6 'damping' matrix where each diagonal element is of approximately the same order of magnitude as the expected variance of each parameter. A initial estimation of model values ($m_{\text{first}} = [0.15; 0.53; 37; 0.27; 24; 0.082]$), yields $v(t)$ from Eq. (2), and d_{res} is calculated from $GV(t) - v(t)$. The G matrix is calculated from partial derivatives of Eq. (2) with parameters of m_{first}, and m_{pert} is

calculated from Eq. (3). Finally, a new m_{first} is set equal to $m_{first}+m_{pert}$ and the algorithm repeats. This iterative process occurs until the solution reaches equilibrium or ten iterations. The final model parameters are recorded for each data point.

2.4. Noise and uncertainty

The curve-fitting formula, as written, assumes that all data points are equally valid and therefore must be assigned the same weight. However, a pixel with clouds or snow cover could produce inaccurate SMA results (Small, 2004) and thus invalid points for the model. Rather than eliminating these points (such as White et al., 1997 and Zhang et al., 2003), we use the error of SMA results and temporal thermal anomalies (from Landsat thermal infrared data) to detect and down-weight the importance of potentially cloud-covered points. The inverse modeling method allows the construction of a diagonal uncertainly matrix (C_{noise}), usually filled with a parameterization of data noise (Menke, 1989). In this implementation, the C_{noise} matrix is filled with the sum of SMA RMSE and an estimation of the likelihood of cloud cover from thermal characteristics (see next section). High RMSE increases data point uncertainty, as do SMA results with green vegetation abundances (GV)<0. Each addition to the C_{noise} matrix reduces the importance of the associated data point to the curve fit.

2.5. Thermal analysis and cloud detection

To find thermal anomalies, we followed a detection method which depends on predictably changing surface temperatures. On average, satellite detected land surface temperatures (LST) should follow patterns of insolation. Although LST displays variability in both time and space, the temporal pattern should trace a sinusoid. Rapid negative deviations from a sinusoidal pattern in temperate regions are indicative of cloud cover. Drawing from principles established in Cayula and Cornillon (1996) and revisited in Fisher and Mustard (2004), cloud-covered pixels were detected as an absolute distance from expected LST (Fig. 2a). For each date, the Landsat thermal infrared band 6 (high gain in ETM+) was converted into radiance and then LST with a uniform emissivity of one (see Fisher and Mustard, 2004, for conversion method). LST errors from incorrect emissivity are small in comparison to annual temperature and cloud cover flux. Detected LST was fit with a three-parameter sinusoid:

$$T(t) = T_{mean} + T_{amp}\cdot\sin\left(2\pi/365\cdot\left(t - T_{phase}\right)\right) \quad (4)$$

mean annual temperature (T_{mean}), amplitude (T_{amp}), and phase-shift (in days: T_{phase}) were all solved with an inverse model for each pixel. For each iteration of the fitting procedure, residuals of $T(t)-\mathrm{LST}>0$ were assigned a greater weight than $T(t)-\mathrm{LST}<0$, driving the sinusoidal fit towards a maximum envelope solution. The value of $|T(t)-LST(t)|$ (in °C) was scaled by 20%, and added to the C_{noise} matrix to reduce the importance of thermally anomalous data.

The C_{noise} diagonal matrix is constructed such that each data point has a noise estimate, approximately of the same order of magnitude as the SMA RMSE error (0–1). Cloud covered points have both a high RMSE and a very high thermal error, and thus are assigned a high value in the C_{noise} matrix. The weighting matrix (W) from Eq. (3) is simply the inversion of the C_{noise} matrix, such that data points with high error are assigned low weights in the matrix inversion. The final sigmoid curve solution thus is determined by the goodness of fit of the SMA, thermal, and sigmoid models (Fig. 2). The final curve-fit solutions are not sensitive to the exact parameterization of noise or the exact values of the damping matrix in Eq. (3). However, erroneous data points must be significantly down-weighted (this paper provides a conservative weighting scheme) to reduce the impact of atmospheric variability on the phenological estimations. For example, a cloud covered forest in mid-summer, without down-weighting, will draw the curve down inordinately. The down-weighting presented in this paper creates significantly cleaner final results without atmospheric artifacts. This same problem impacts all satellite-based phenological studies.

2.6. Accounting for interannual variability

Interannual climate variability and temperature fluctuations alter phenological characteristics. Warm springtime temperatures yield early bud-break and leafing, for which we must account if we are to use multiple years of data in a single fit. The method presented here requires the direct comparison of greenness between different years, and thus we present a system in which we introduce a time lag into Eq. (2). These lags (b_1 and b_2) are specific to each year such that the curve passing through all scenes from a given year will be phase shifted from the global mean to match the characteristics of that year while holding all other parameters constant. This method reduces variance due only to interannual variability while preserving spatial and annual patterns. With the available amount of data, these offsets are assumed to be uniform for the entire scene. If the offsets were calculated for each individual pixel, the curve-fit would have 63 parameters rather than six, and the results would be poorly constrained.

The new form of the equation is:

$$v(t) = v_{min} + v_{amp}\left(\frac{1}{1+e^{m_1+m_2(t-b_1)}} - \frac{1}{1+e^{m_3+m_4(t-b_2)}}\right) \quad (5)$$

where b_1 and b_2 are values (in units of days) specific to each year which control how early or late that *entire* scene falls. Thus, if in 2001, budbreak began 8 days earlier than average, the value of b_1 would be -8 for all data points obtained in 2001. The values of b_1 do not impact senescence, because the curve is shifted, rather than the data points. There are 18 set values of b_1 and b_2, corresponding to the years 1984–2002. The values of b_1 and b_2 are obtained by simultaneously fitting 80 spatially dispersed EDF pixels, allowing all other parameters to shift, but holding b_1 and b_2 constant over all pixels. Table 1 indicates the number of days the greenup curve was shifted to find a best fit. Since greenup and senescence were not observed in all years, b_1 and b_2 do not represent

Table 1
Phase offset factors b_1 (greenup) and b_2 (senescence) calculated for each year

Year	b_1	Number of scenes ($50 \leq$ DOY < 200)	b_2	Number of scenes ($200 \leq$ DOY < 300)
1984	0.9	1	−2.6	3
1985	0.7	1	−3.2	3
1986	–	–	−2.5	1
1987	0.0	3	−1.9	1
1988	–	–	–	–
1989	0.0	1	−3.9	3
1990	1.1	1	–	–
1991	0.0	1	0.4	1
1992	–	–	–	–
1993	−0.6	1	−0.2	1
1994	4.5	1	–	–
1995	–	–	–	–
1996	–	–	–	–
1997	–	–	−0.5	2
1998	−0.2	1	–	–
1999	0.0	1	0.1	1
2000	1.7	1	9.4	3
2001	−6.9	7	4.4	3
2002	−1.1	2	0.3	1

A positive b value is a phenologically delayed year. All offsets are relative to the dataset mean, and cannot be used to represent actual values of interannual variability. The number of scenes in each year which influenced the b parameter is estimated in adjoining columns. Scenes which fell between DOY 50 and 200 are likely to be more influential in b_1, whereas scenes falling between DOY 200 and 300 will influence b_2 more strongly. The closer a scene falls to the curve half-max, the more influential it will be in determining the annual phenology.

comprehensive interannual variability, but instead allow different years to be compared and improves the robustness of the model.

2.7. Field observations and validation

Field validations were conducted throughout the 2005 greenup (April 7th through May 18th) along transects in Arcadia Wildlife Management Area (WMA) in RI, and Douglas Forest and Buck Hill WMA at the CT/MA/RI tristate junction. Transects were selected to cut across strong leaf onset gradients predicted by the Landsat model. Ground observations took into account species, topography, soil conditions, hydrology, and land-use history. The transects traversed 50-year-old forests dominated by red oak (*Quercus rubra*), with lower concentrations of white oak (*Quercus alba*) and red maple (*Acer rubrum*). Trace canopy level sassafras (*Sassafras albidum*), beech (*Fagus grandiflora*), white birch (*Betula papyrifera*), and white pine (*Pinus strobus*) were observed as well. Typically, forests graded rapidly into eastern hemlock (*Tsuga canadensis*) and white pine after the latest leaf onset date in the gradient. Ground transects did not extend into areas masked as coniferous or mixed forests.

Optical estimates of field phenological conditions along the transects provided a validation of satellite predicted phenology. Multiple photographs of canopy and understory conditions were obtained at each transect point throughout the season and graded by four independent observers. The 355 randomized photographs were marked on a 0–4 scale of phenological development from dormancy to full canopy, respectively (Richardson et al., unpublished). Specific dates and locations were matched to satellite model estimates of phenological development in a 30 m buffer around each transect point. A uniform offset of +7 days was added to the 2005 DOY of observation when matching to the satellite parameters to account for the unusually cool spring in 2005. Fig. 3 indicates a strong relationship (logarithmic fit: $r^2=0.91$) between the model phenological stage and average optical estimate at each location. Each data point in Fig. 3 represents a single location on a specific DOY. Satellite model error represents the first standard deviation of model parameters in 30 m buffer. Optical estimate error is the average of all observers' standard deviation between multiple photographs at each location. The strong relationship indicates that the satellite model from a long Landsat record successfully captures phenological variability as observed on the ground.

2.8. Masking non-deciduous forests

Deciduous plants appear to primarily respond to temperature and photoperiod triggers (Lechowicz, 1984). In both plot-based and satellite observations there are established phenological markers in deciduous species. Although conifers have been shown to exhibit phenologies (Cannell & Smith, 1983; Dougherty, Whitehead, & Vose, 1994) the satellite-observable manifestation of new needle and shoot growth is not as clear as deciduous leaf development. In coarse spatial (kilometer to degree scale) satellite phenology studies, coniferous and mixed forests are difficult to segregate, resulting in compositional uncertainty. The high abundance of pine and hemlock through this region virtually guarantees compositional mixing at coarse scales. In New England EDF, over 85% of forest stands are smaller then 6 km^2 (Foster et al., 1998) and thus coarse satellite studies are likely to include both forest and non-forest. Satellite observations of greenness in non-forest will differ from EDF due to the presence of non-native species planted in urban areas, green lawns in suburban areas, and agricultural plots. The impact of coniferous forest and non-forest cover types on the observation of phenological markers is uncertain, thus we choose to observe deciduous forests only and conservatively mask all other areas. The higher resolution offered by Landsat provides an appropriate platform for locating and isolating pure stands of deciduous forest.

Coniferous forests and urban areas are phenologically distinct from deciduous forests (Duchemin et al., 1999). Conifers maintain a minimum greenness through the winter, while urban and suburban areas are less green at the peak of the growing season. Therefore, a simple mask may be constructed stipulating a lower threshold of average maximum greenness (v_{max}, or $v_{min}+v_{amp}$), and an upper threshold of minimum greenness (v_{min}), where v_{min} and v_{max} are derived from the sigmoid fit. A scatterplot of v_{min} against v_{max} illustrates the linear mixing relationship which separates forest compositions (Fig. 4). A threshold of $v_{min} \leq 0.10$ and

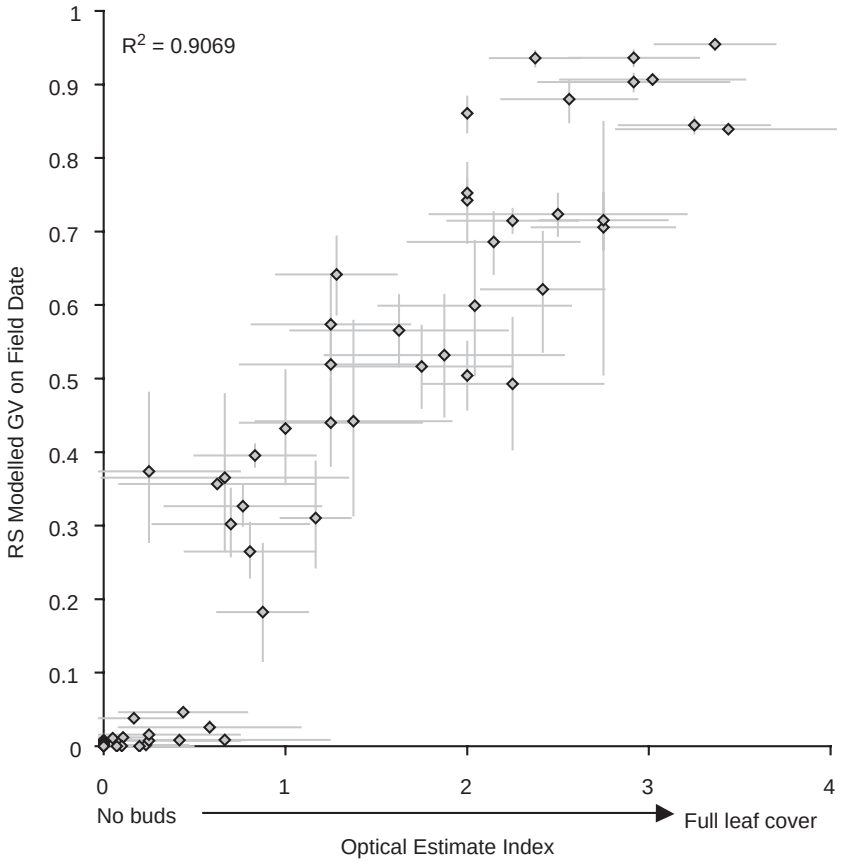

Fig. 3. Validation curve comparing optical estimates from greenup field photographs and green vegetation abundance as modeled with the sigmoid curve from satellite data at the same location on the same DOY (with a 7-day phase shift). Each point represents a multiple observations at a single location on a certain date. Optical estimate error is calculated by averaging the standard deviation of all observers' estimates from multiple photographs at a single location. Curve parameters from pixels within a 30-m buffer of each transect point are calculated, the standard deviation of GV on the date of observation (+7 days) forms the model error.

$v_{max} \geq 0.55$ conservatively isolates deciduous forests more effectively than masks derived from state composition maps. The mask was demonstrated to be sensitive in field tests, identifying pixels with as few as one canopy conifer per pixel (~10% canopy cover).

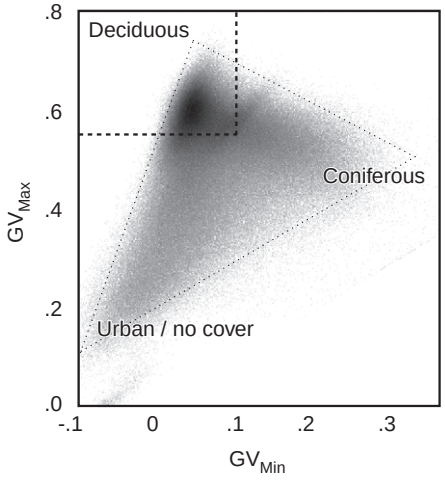

Fig. 4. Scatter plot of GV_{min} vs. GV_{max} demonstrating natural ternary spread of data. Boundaries chosen in this study to conservatively identify deciduous forest are shown. Pixels obtaining average $GV_{max} \geq 0.55$ and $GV_{min} \leq 0.1$ were defined as deciduous forests.

3. Results and discussion

The date of leaf onset was found to have a high degree of spatial variability in southern New England deciduous forests (Fig. 5). Onset ranged from 122 (May 1st) to 163 (June 11th), and had a scene average of 135.16±5.34 with a mode at 134 (May 13th). It is important to note that the absolute date of leaf onset will change annually. The date of leaf onset in this study represents a climatological average, and the broad pattern and relative differences between onset dates across the scene are expected to remain consistent year to year. Although latitudinal gradients are not observed in southern New England, southern CT is largely earlier than both central MA and coastal RI, as well as Cape Cod and Martha's Vineyard in the south of the image. The latest greenup occurs on the exposed south coast and the Islands, and continues up in a sinuous pattern through the CT/RI border into central MA.

Large temporal gradients in leaf onset which occur in small special scales are seen throughout central MA and in the CT/RI border. These patterns are unexpected and may demonstrate the apparently undocumented phenomenon (at this scale) of

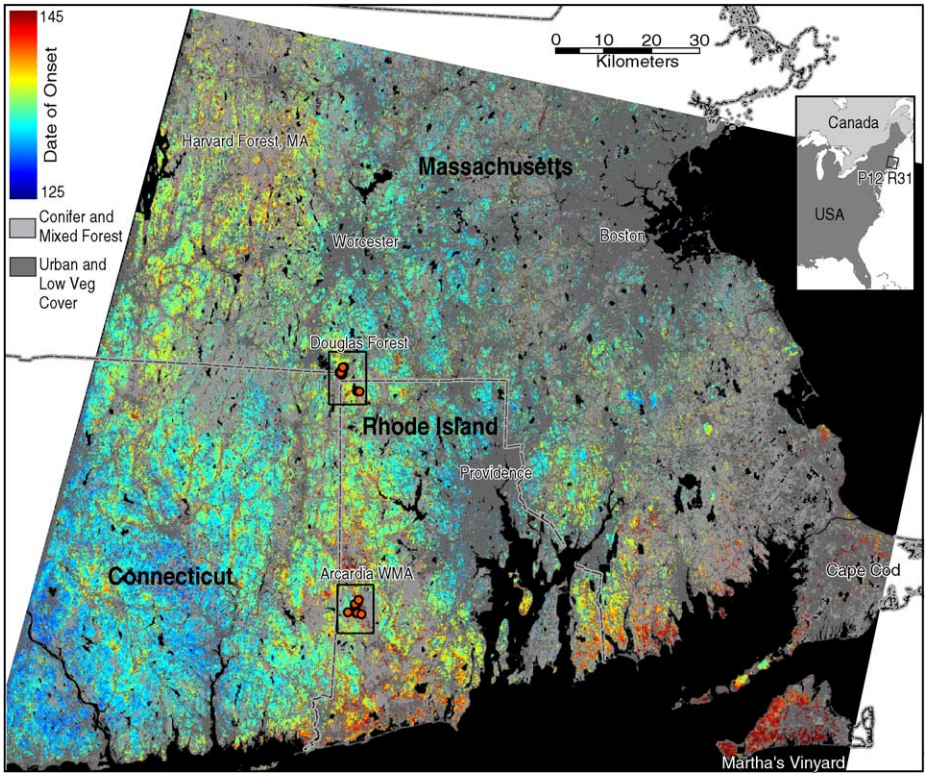

Fig. 5. Green leaf onset over southern New England. Cooler colors indicate earlier onset and leaf-out in deciduous forests, warmer colors are later onset and canopy development. Conifer and mixed forests and urban areas are not colored. The latest onset dates occur on the south and east coasts which experience cool spring temperatures. Broad spatial patterns appear to be controlled by climate gradients, distance to coastline, and elevation. Late onset through RI/CT border is primarily a function of extensive cold air valleys. Topography throughout the scene is subtle.

persistent, phenologically important microclimates. Fig. 6 (a detail of Fig. 5) suggests that the date of leaf onset varies smoothly by over 2 weeks at very fine spatial scales (<1 km). The 2-week differences demonstrated here are of the same magnitude as the broad-scale variability across the entire region.

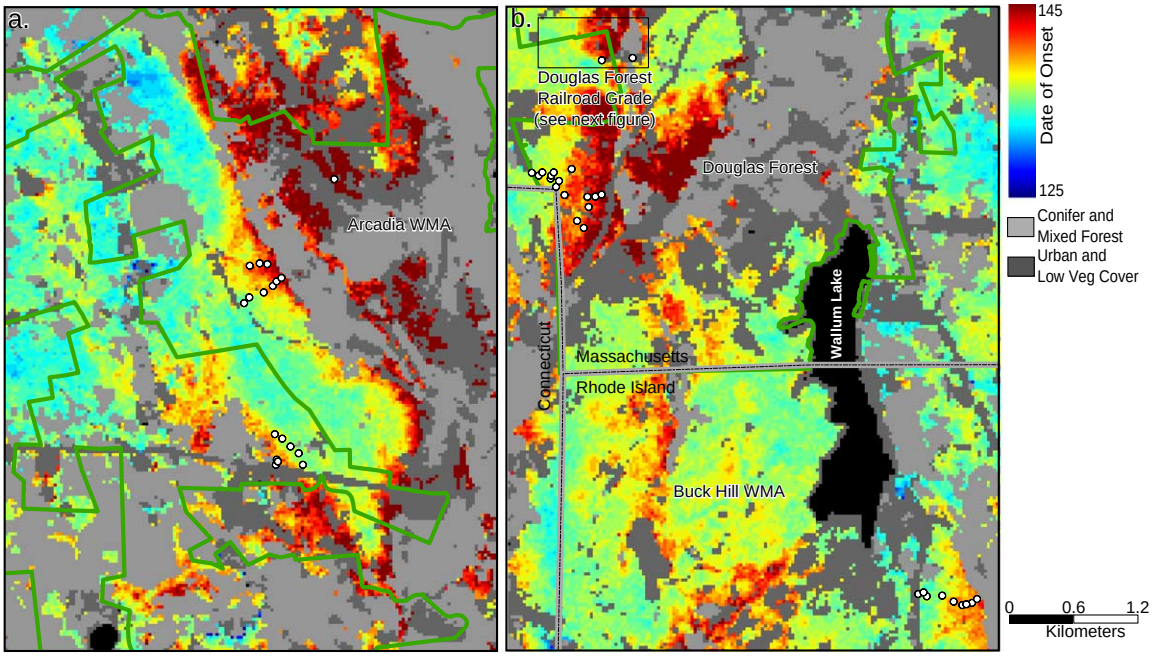

Fig. 6. Green leaf onset in (a) Arcardia, Rhode Island and (b) Douglas Forest, Massachusetts, and Buck Hill WMA, Rhode Island. Color scheme is the same as Fig. 5. Transects (marked in white circles) were designed to cut across steep leaf onset gradients. Later leaf onset dates are strongly correlated with topography in this region; lower topography delays onset due to cold air drainage.

3.1. Growing season variability at small scales-microclimates

The strong leaf onset date gradients predicted by the Landsat phenological model were observed in ground transects. Phenological development was consistent with predictions in all tested scenarios. Over a distance of less than 500 m, more than a 2-week delay could be observed in forests with similar composition, age, and structure. In most cases, emergence of understory foliage (primarily red maple and blueberry—*Vaccinium* spp.) was coincident with canopy budburst. Spatial patterns of satellite observed onset dates were not correlated with species composition, forest structure (height, gap distribution, stem density, or density of the shrub layer), surface hydrology, slope, or soil type. However, later onset dates consistently and predictably occurred at locally slightly lower elevations (<50 m difference) as demonstrated in Fig. 7. Local elevation was derived from the Shuttle Radar Topography Mission (SRTM) 1-arcsec (30m) dataset (±10 m vertical accuracy) and, when available, MassGIS orthophoto-derived digital terrain models (±3 m) and Rhode Island Star3i synthetic aperture radar digital elevation model data (±2.5 m).

Leaf onset trends are tightly coupled to local elevation at each site (Fig. 8). There is a slight delay in the earliest date of onset in each transect as elevation increases between sites, but there is a far more dramatic delay in leaf onset dates with local elevation gradients. All transects indicated a strongly correlated negative relationship between elevation and the date of leaf onset (total sample $r^2=0.82$). Variability in the onset date metric was far greater at the transect scale than between distant locations (~50 km from Douglas Forest to Arcadia WMA). In

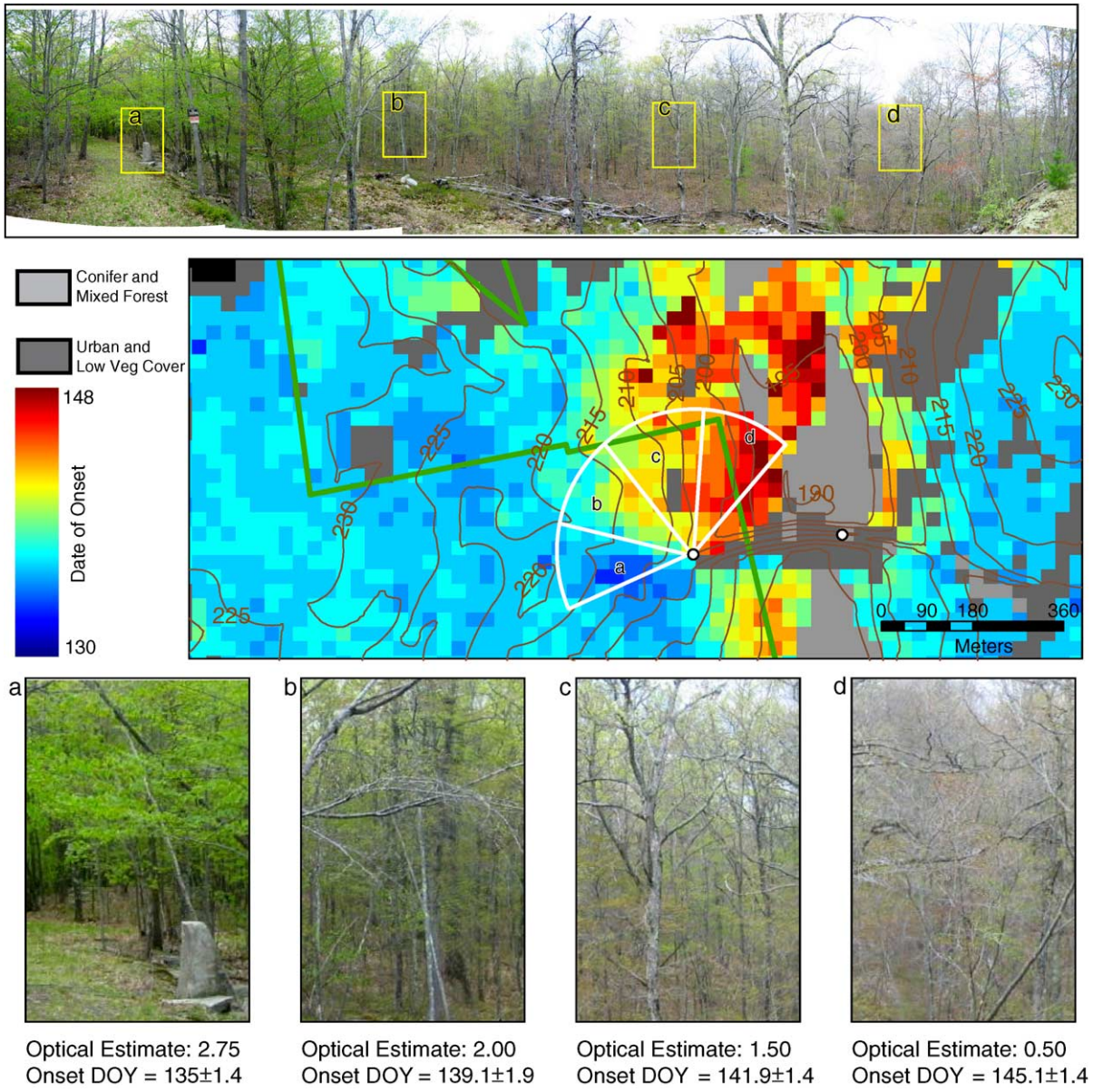

Fig. 7. The relationship between topography and leaf onset at Douglas Forest. The 160° panoramic photograph was obtained on a railroad grade above a shallow valley on May 18, 2005. From left to right, the forest is phenologically later (optical estimates from 3 to 0, respectively). In the map below the photograph, a gradient in onset of over 2 weeks is predicted by the Landsat product. The topography in this area is 30 m over a ~500 m distance.

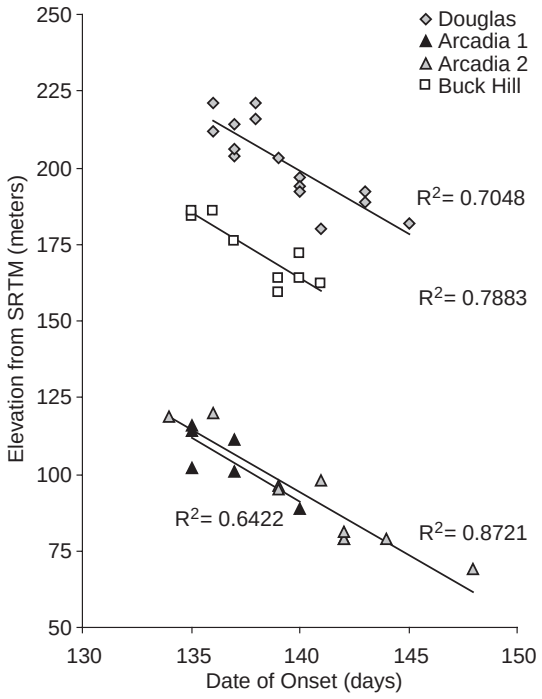

Fig. 8. Scatterplot of the date of green leaf onset against elevation along each transect. Local topography strongly influences the date of onset at the field sites in an inverse relationship to that which is normally observed.

these steep gradient areas, every 4.16 m of elevation loss resulted in an average onset delay of 1 day.

The strong relationship between onset date and topography may be described by seasonally persistent spring microclimates formed from cold air drainage (Pellikka, 2001). In a classical scenario, phenological development is later at higher elevations due to the adiabatic cooling with elevation (Bolstad et al., 1998; Fitzjarrald, Acevedo, & Moore 2001). In the circumstances described here, cold air formed by radiative cooling on still nights moves down slope along a density gradient and is trapped in the surrounding valleys (Bolstad et al., 1998; Mahrt et al., 2001; Morecroft et al., 1998; Soler, Infante, & Buenestado, 2002). Bolstad et al. (1998) observed that cold air drainage is most pronounced during the early spring, a period highly influential in phenological timing. The cumulative effect of colder air trapped in the valleys is to delay phenology in the valley by reducing the sum growing degree days. Delays of greenup imposed by cold air drainage at such a fine scale naturally raises questions about broader scale satellite phenologies, comparing between field-scale long-term observations (Richardson et al., unpublished; Roetzer et al., 2000; Schaber & Badeck, 2003; Wolfe et al., 2005), and scaling-up phenological field observations to regional and global scales (Chuine et al., 2000; Jenkins et al., 2002; White et al., 1997).

3.2. Growing season variability and regional patterns

Broad regional patterns of leaf onset date variability in southern New England (Fig. 5) are spatially coherent and realistic for spring climatological patterns. In southern New England, ocean sea surface temperatures lag mainland climatology (Fisher & Mustard, 2004). The south coast, Cape Cod, and Martha's Vineyard are influenced by cooler oceanic temperatures in the spring. The large swaths of late onset dates across central MA and the RI/CT border are largely controlled by regional and local topography (see above section). The regional patterns (Fig. 5) are similar to those presented by Zhang et al. (2003) using 1 km MODIS data in the same region. In their work, the 'greenup onset' metric (describing the inflection point of the greenup curve) indicates a phenological delay on Cape Cod relative to the mainland of approximately 20 days. Similarly, the 'maturity onset' metric (the end up the greenup curve) also shows a later leaf onset date on the south coast in RI and MA compared to CT, and the same 15–20 day delayed pattern extending up the CT-RI border into central MA. However, at the 1 km resolution, local topographic patterns and microclimates causing the apparently anomalous delay are obscured.

3.3. Urban heat island detection

Numerous studies, both field scale and at the satellite scale, suggest that urban areas locally increase evening springtime sensible heat, causing urban heat islands (UHI) (Arnfield, 2003; Block, Keuler, & Schaller, 2004; Henry et al., 1989; Kim, 1992; Streutker, 2003). The influence of urban heat should be detectable in phenology as an earlier leaf onset when observing deciduous forests. Two studies have indicated the presence of phenologically important urban heat islands using different data series. White et al. (2002) explores Atlantic coast urban areas using AVHRR NDVI MVC data, and utilizes a very coarse spatial scale (in 1° pixels). The 14-day temporal uncertainty from the MVC is longer than expected variance in onset dates due to urban heat, the grid size is much larger than the expected spatial extent or influence of an urban area, and the model is sensitive to small amounts of noise. Zhang et al. (2004a,b) uses higher spatial resolution (1 km) MODIS data and a logistic growth model (similar to this study) to observe the impact of urban heat on phenology. Zhang et al.'s onset metric is aggregated into 2–5 km concentric buffers around urban areas. Unfortunately, aggregating over wide buffers with coarse pixel sizes cannot distinguish suburban lawn and coniferous signals from changes in native forests. In contrast, at the Landsat scale, we are able to exclusively observe deciduous forests. The mask thresholds chosen in this research exclude urban and suburban areas, and to observe phenology patterns in peri-urban deciduous forests only.

Thirty-five kilometer radial transects at 5° intervals were extended from central Providence, and the date of deciduous forest leaf onset were averaged in 300 m bins along each spoke. We found that there is a power relationship between distance from an urban core and onset date (Fig. 9), similar to the inverse exponential relationship found by Zhang et al. (2004a,b). This relationship between urban distance and onset suggests that urban areas impact local climatological patterns which are reflected in peri-urban phenological characteristics. Based on this trend, we would expect to observe a UHI

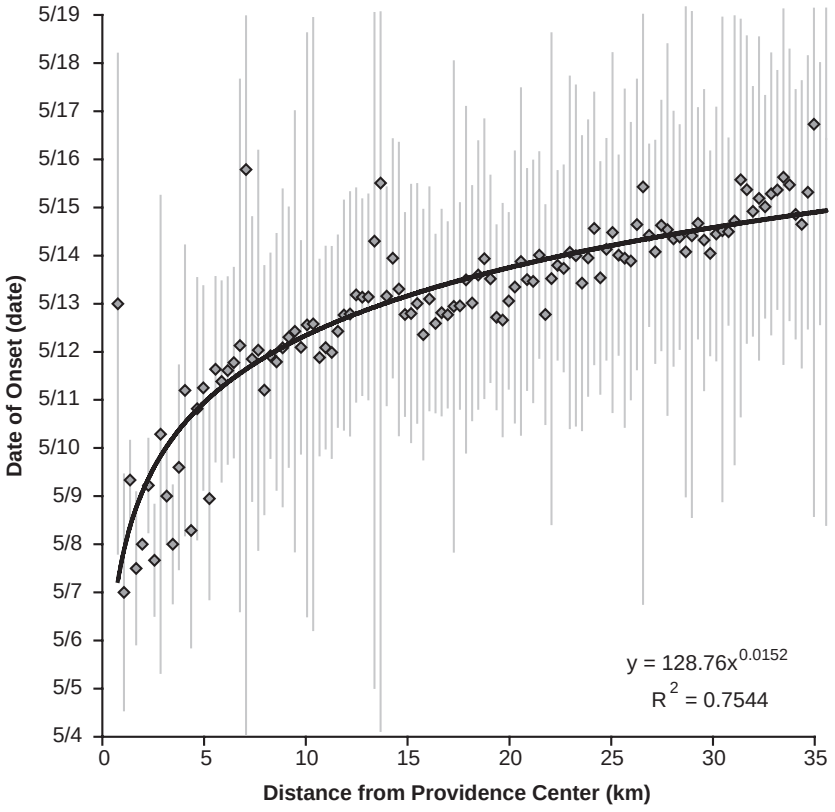

Fig. 9. Green leaf onset as a function of distance from Providence urban core. All deciduous pixels within 300 m concentric bins are averaged. Error bars are the standard deviation of all valid pixels onset date. Urban heat islands appear to accelerate the date of onset by approximately 1 week. These results are similar to those presented in Zhang.

extending from 5 to 10 km from the urban core of Providence, RI. This first order approximation does not differentiate asymmetric influences from Narragansett Bay to the south, non-concentric urban development, and topographic differences in all directions from Providence. By isolating deciduous fragments in urban environments at the 30-m scale, rather than aggregating phenological characteristics over an entire urban area, we rule out forest composition and anthropogenic features (such as lawns and horticulture) as signal modifiers. Ensuring that an observed phenology signal is generated by pure deciduous forests is an important step in understanding the interplay of anthropogenic heat and earlier onset dates.

3.4. Caveats and methodological uncertainty

It is important to note that this research draws on a very large Landsat database. However, repetition of this research emphasizing the date of onset in particular is possible with a much smaller Landsat database covering the time-period from thaw to maximum leaf canopy cover and a slightly modified algorithm. In the northeast United States, spring greenup is often obscured by clouds, and so obtaining a relatively cloud-free database is a difficult endeavor. Although the methodology becomes more accurate with larger numbers of scenes, the algorithm which we present is highly robust to sparse data during the transition seasons. The methodology detailed in this research may be readily extended to other regions and even other satellite platforms with different greenness metrics. The calculation of NDVI does not provide the error bounds required for this weighted fitting technique.

The use of the spectral mixture analysis in this method requires a proper spectral calibration between scenes, and errors may result in inappropriately calculated areal leaf cover. However, the vegetation fraction is a robust measure of vegetation density, and small errors in this calculation would not be expected to unduly impact the relative timing of onset as calculated in the curve-fit. In addition, significant changes in forest structure over time may also alter the derived metrics, as would local variations in water availability, infestation, or disease. The curve fitting mechanism proposed in this research acts as a low-pass filter, and assumes only one cycle of greening per season. The single-cycle model is accurate for deciduous forests, but in the current form may not represent more complex changes in other vegetation communities. Further research would be required to determine phenological curve shapes for other ecosystems.

4. Conclusion

The Landsat scale of phenological observation provides an effective scaling mechanism between intensive plot-scale ground studies of phenology and large scale phenological mapping. The fine spatial scales of phenological variability noted in this research are lost in aggregation. Due to

dissimilarities between urban, coniferous, and deciduous spatial patterns, we emphasize here that coarse spatial scale (AVHRR and MODIS) phenological studies must rigorously account for forest and ground cover composition to accurately report on satellite-observed phenology.

The temporal variability in the dates of leaf onset observed in this study occurred in a relatively narrow window; the onset date of 95% of all EDF fell within a 13-day window (DOY 128–145), and 99% occurred in a 28 day window (DOY 125–153). Therefore, we caution that satellite-based phenological studies must have accurate knowledge of the acquisition DOY for each pixel. Datasets of AVHRR and MODIS MVC vegetation indices (often binned in 8-day to 1-month bins) unfortunately loose critical temporal data required to model phenological processes. Phenological studies utilizing composite datasets (DeFries et al., 1998; Ebata & Tateishi, 2001; Jenkins et al., 2002; Justice et al., 1985; Moulin et al., 1997; Myneni et al., 1997; Reed et al., 1994; Schwartz & Reed, 1999; Schwartz et al. 2002; White et al., 2002; Zhang et al., 2003) must take into account the high degree of temporal uncertainty imposed by the compositing methodology as currently implemented (Holben, 1986). Similarly, studies which use temporal interpolation to fill missing data (Reed et al., 1994; Viovy & Arino, 1992; White et al., 1997, 2002; Zhang et al. 2003) should be aware that additional weight given to the bounding points which guide the interpolation will be reflected in the final product. In particular, methods which rely on single values (minima, maxima, and midpoints) to determine a phenological metric (Ebata & Tateishi, 2001; Jenkins et al., 2002; Moulin et al., 1997; Reed et al., 1994; Schwartz et al., 2002; White et al., 1997, 2002) risk recording noise rather than a value which reflects the larger data set. Phenological fitting methods which are robust to noise (Jönsson & Eklundh, 2002; Richardson et al., unpublished; Zhang et al., 2003) effectively overcome some of the difficulties imposed by sparse datasets. In this research we find that in the Douglas Forest/Buck Hill region, the addition of 20% random noise to the calculated GV time series results in ±1.8 days at onset and ±3.0 days at offset in deciduous forests. Therefore, we are confident that the trends we observe are significant and robust under excessive noise. We strongly encourage temporal information to be retained and utilized to the fullest extent possible in future satellite phenology research.

The significant spatial variability at the start of the growing season in the eastern deciduous forests of southern New England has numerous potential implications for phenological research and ecosystem models. Phenological forcing by microclimates and cool air pockets in shallow topography suggests that extrapolating climatological and carbon flux values from isolated towers may require a more comprehensive understanding of local persistent climatological conditions. The combined satellite and ground evidence of phenologically important persistent cold air drainage provides an intriguing natural experiment. Compositionally uniform forests extending into the cool air drainage may be observed under slightly different climate conditions. An opportunity is now available to track phenological triggers over contiguous forest stands. At a small scale, we may observe the impact of gradational climate changes on the phenology and subsequent carbon flux in indigenous deciduous forests.

Acknowledgements

We would like to thank the Rhode Island Department Division of Forest Environment and the Massachusetts Department of Conservation and Recreation where ground validation was performed. We extend thanks to Donald Forsyth for his assistance in algorithm development and error checking, Andrew Richardson for insightful comments, and four anonymous reviewers with constructive critiques. We appreciate the elevation and auxiliary datasets provided by the Massachusetts Office of Geographic and Environmental Information (MassGIS), NASA's Earth Science Enterprise and Earthwatch Incorporated (Star-3*i* data), and the NASA's Shuttle Radar Topography Mission (SRTM) program. Research was partially supported by the Department of Geological Sciences at Brown University. The Landsat database was obtained under grants from the University of Rhode Island /NOAA Cooperative Marine and Education Research Program, the National Oceanographic Partnership Program, NASA Land Use and Land Cover Change, and the Rhode Island Department of Environmental Management.

References

Aber, J. D., Ollinger, S. V., Federer, C. A., Reich, P. B., Goulden, M. L., Kicklighter, D. W., et al. (1995). Predicting the effects of climate change on water yield and forest production in the Northeastern United States. *Climate Research*, *5*, 207–222.

Adams, J. B., Smith, M. O., & Gillespie, A. R. (1993). Imaging spectroscopy: Interpretation based on spectral mixture analysis. In C. M. Pieters, & P. A. J. Englert (Eds.), *Remote geochemical analysis: elemental and mineralogical composition* (pp. 145–166). Cambridge, England: Press Syndicate of University of Cambridge.

Arnfield, A. J. (2003). Two decades of urban climate research: A review of turbulence, exchanges of energy and water, and the urban heat island. *International Journal of Climatology*, *23*, 1–26.

Arora, V. K., & Boer, G. J. (2005). A parameterization of leaf phenology for the terrestrial ecosystem component of climate models. *Global Change Biology*, *11*, 39–59.

Asner, G. P. (1998). Biophysical and biochemical sources of variability in canopy reflectance. *Remote Sensing of Environment*, *64*, 234–253.

Badhwar, G. D. (1984). Use of LANDSAT-derived profile features for spring small-grains classification. *International Journal of Remote Sensing*, *5*, 783–797.

Block, A., Keuler, K., & Schaller, E. (2004). Impacts of anthropogenic heat on regional climate patterns. *Geophysical Research Letters*, *31*, L12211.

Bolstad, P. V., Swift, L., Collins, F., & Régnière, J. (1998). Measured and predicted air temperatures at basin to regional scales in the southern Appalachian Mountains. *Agricultural and Forest Meteorology*, *91*, 161–176.

Bouzille, J. B., Bonis, A., Clément, B., & Godeau, M. (1997). Growth patterns of *Juncus gerardi* clonal populations in a coastal habitat. *Plant Ecology*, *132*, 39–48.

Cannell, M. G. R., & Smith, R. I. (1983). Thermal time, chill days, and prediction of budburst in *Picea sitchensis*. *Journal of Applied Ecology*, *20*, 951–963.

Cao, M., & Woodward, F. I. (1998). Dynamic responses of terrestrial ecosystem carbon cycling to global climate change. *Nature*, *393*, 249–252.

Cayula, J. F., & Cornillon, P. (1996). Cloud detection from a sequence of SST images. *Remote Sensing of Environment*, *55*, 80–88.

Chuine, I., Cambon, G., & Comtois, P. (2000). Scaling phenology from the local to the regional level: Advances from species-specific phenological models. *Global Change Biology*, *6*, 943–952.

Côté, B., Hendershot, W. H., Fyles, J. W., Roy, A. G., Bradley, R., Biron, P., et al. (1998). The phenology of fine root growth in a maple-dominated ecosystems: Relationships with some soil properties. *Plant and Soil*, *201*, 59–69.

DeFries, R. S., Hansen, M., Townshend, J. R. G., & Sohlberg, R. (1998). Global land cover classifications at 8 km spatial resolution: The use of training data derived from Landsat imagery in decision tree classifiers. *International Journal of Remote Sensing*, *19*, 3141–3168.

Dixon, K. R. (1976). Analysis of seasonal leaf fall in north temperate deciduous forests. *Oikos*, *27*, 300.

Dougherty, P. M., Whitehead, D., & Vose, J. M. (1994). Environmental influences on the phenology of pine. *Ecological Bulletins*, *43*, 64–75.

Duchemin, B., Goubier, J., & Courrier, G. (1999). Monitoring phenological key stages and cycle duration of temperate deciduous forest ecosystems with NOAA/AVHRR data. *Remote Sensing of Environment*, *67*, 68–82.

Ebata, M., Tateishi, R. (2001). Phenological stage monitoring in Siberia by using NOAA/AVHRR data. *22nd Asian Conference on Remote Sensing, Singapore, Centre for Remote Imaging, Sensing and Processing (CRISP).*

Elmore, A. J., Mustard, J. F., Manning, S. J., & Lobell, D. B. (2000). Quantifying vegetation change in semiarid environments: Precision and accuracy of spectral mixture analysis and the normalized difference vegetation index. *Remote Sensing of Environment*, *73*, 87–102.

Fisher, J. I., & Mustard, J. F. (2004). High spatial resolution sea surface climatology from Landsat thermal infrared data. *Remote Sensing of Environment*, *90*, 293–307.

Fitzjarrald, D. R., Acevedo, O. C., & Moore, K. E. (2001). Climatic consequences of leaf presence in the Eastern United States. *Journal of Climate*, *14*, 598–614.

Foster, D. R., Motzkin, G., & Slater, B. (1998). Land-use history as long-term broad-scale disturbance: Regional forest dynamics in Central New England. *Ecosystems*, *1*, 96–119.

Goetz, S. J., & Prince, S. D. (1996). Remote sensing of net primary production in boreal forest stands. *Agricultural and Forest Meteorology*, *17*, 149–179.

Henry, J. A., Dicks, S. E., Wetterqvist, O. F., & Roguski, S. J. (1989). Comparison of satellite, ground-based, and modeling techniques for analyzing the urban heat island. *Photogrammetric Engineering and Remote Sensing*, *55*, 69–76.

Holben, B. N. (1986). Characteristics of maximum-value composite images from temporal AVHRR data. *International Journal of Remote Sensing*, *7*, 1417–1434.

Hollinger, D. Y., Aber, J. D., Dail, B., Davidson, E. A., Goltz, S. M., Hughes, H., et al. (2005). Spatial and temporal variability in forest-atmosphere CO_2 exchange. *Global Change Biology*, *10*, 1689.

Hunter, A. F., & Lechowicz, M. J. (1992). Predicting the timing of budburst in temporate trees. *The Journal of Applied Ecology*, *29*, 597–604.

Jenkins, J. P., Braswell, B. H., Frolking, S. E., & Aber, J. D. (2002). Detecting and predicting spatial and interannual patterns of temperate forest springtime phenology in the eastern U.S. *Geophysical Research Letters*, *29*, 54.

Jönsson, P., & Eklundh, L. (2002). Seasonality extraction by function fitting to time-series of satellite sensor data. *IEEE Transactions on Geoscience and Remote Sensing*, *40*, 1824–1832.

Justice, C. O., Townshend, J. R. G., Holben, B. N., & Tucker, C. J. (1985). Analysis of the phenology of global vegetation using meteorological satellite data. *International Journal of Remote Sensing*, *6*, 1271–1318.

Kato, S., & Komiyama, A. (2002). Spatial and seasonal heterogeneity in understory light conditions caused by differential leaf flushing of deciduous overstory trees. *Ecological Research*, *17*, 687–693.

Kim, H. H. (1992). Urban heat island. *International Journal of Remote Sensing*, *13*, 2319.

Lechowicz, M. J. (1984). Why do temperate deciduous trees leaf out at different times? Adaptation and ecology of forest communities. *The American Naturalist*, *124*, 821–842.

Menke, W. (1989). *Geophyiscal Data Analysis: Discrete Inverse Theory*. San Diego: Academic Press.

Mahrt, L., VIckers, D., Nakamura, R., Soler, M. R., Sun, J., Burns, S., et al. (2001). *Shallow drainage flows. Boundary-layer meteorology*, *101*, 243–260.

Morecroft, M. D., Taylor, M. E., & Oliver, H. R. (1998). Air and soil microclimates of deciduous woodland compared to an open site. *Agricultural and Forest Meteorology*, *90*, 141–156.

Moulin, S., Kergoat, L., Viovy, N., & Dedieu, G. (1997). Global-scale assessment of vegetation phenology using NOAA/AVHRR satellite measurements. *American Meteorological Society*, *10*, 1154–1170.

Mustard, J. F., & Sunshine, J. M. (1999). Spectral analysis for earth science: Investigations using remote sensing data in remote sensing for the earth sciences. In A. Rencz (Ed.), *Manual of Remote Sensing* (pp. 251–307). New York: J. Wiley and Sons.

Myneni, R., Keeling, C. D., Tucker, C. J., Asrar, G., & Nemani, R. R. (1997). Increased plant growth in the northern high latitudes from 1981 to 1991. *Nature*, *386*, 698–702.

NASA, Landsat Project Science Office. (2003). Landsat 7 Science Data Users Handbook, NASA at http://ltpwww.gsfc.nasa.gov/IAS/handbook/handbook_toc.html

Parker, G. G., & Tibbs, D. J. (2004). Structural phenology of the leaf community in the canopy of a *Liriodendron tulipifera* L. forest in Maryland, USA. *Forest Science*, *50*, 387–397.

Pellikka, P. (2001). Application of vertical skyward wide-angle photography and airborne video data for phenological studies of beech forests in the German Alps. *International Journal of Remote Sensing*, *22*, 2675–2700.

Potter, C., Klooster, S., Myneni, R., Genovese, V., Tan, P. N., & Kumar, V. (2003). Continental-scale comparisons of terrestrial carbon sinks estimated from satellite data and ecosystem modeling 1982–1998. *Global and Planetary Change*, *39*, 201–213.

Rastetter, E. B., King, A. W., Cosby, B. J., Hornberger, G. M., O'Neill, R. V., & Hobbie, J. E. (1992). Aggregating fine-scale ecological knowledge to model coarser-scale attributes of ecosystems. *Ecological Applications*, *2*, 55–70.

Reed, B. C., Brown, J. F., VanderZee, D., Loveland, T. R., Merchant, J. W., & Ohlen, D. O. (1994). Measuring phenological variability from satellite imagery. *Journal of Vegetation Science*, *5*, 703–714.

Rötzer, T., Grote, R., & Pretzsch, H. (2004). The timing of bud burst and its effect on tree growth. *International Journal of Biometeorology*, *48*, 109–118.

Running, S. W., & Nemani, R. R. (1991). Regional hydrologic and carbon balance responses of forests resulting from potential climate change. *Climate Change*, *19*, 349–368.

Schaber, J., & Badeck, F. W. (2003). Physiology-based phenology models for forest tree species in Germany. *International Journal of Biometeorology*, *47*, 193–201.

Schwartz, M. D., & Reed, B. C. (1999). Surface phenology and satellite sensor-derived onset of greenness: an initial comparison. *International Journal of Remote Sensing*, *20*, 3451–3457.

Schwartz, M. D., Reed, B. C., & White, M. A. (2002). Assessing satellite-derived start-of-season measures in the conterminous USA. *International Journal of Climatology*, *22*, 1793–1805.

Seiwa, K. (1999). Changes in leaf phenology are dependent on tree height in acer mono, a Deciduous broad-leaved tree. *Annals of Botany*, *83*, 355–361.

Small, C. (2004). The Landsat ETM+ spectral mixing space. *Remote Sensing of Environment*, *93*, 1–17.

Soler, M. R., Infante, C., & Buenestado, P. (2002). Observations of nocturnal drainage flow in a shallow gully. *Boundary-Layer Meteorology*, *105*, 253–273.

Song, C., Woodcock, C. E., & Li, X. (2002). The spectral/temporal manifestation of forest succession in optical imagery: The potential of multitemporal imagery. *Remote Sensing of Environment*, *82*, 285–302.

Streutker, D. R. (2003). Satellite-measured growth of the urban heat island of Houston, Texas. *Remote Sensing of Environment*, *85*, 282–289.

Thomas, A., Byrne, D., & Weatherbee, R. (2002). Coastal sea surface temperature variability from Landsat infrared data. *Remote Sensing of Environment*, *81*, 262–272.

Viovy, N., & Arino, O. (1992). The Best Index Slope Extraction (BISE): A method for reducing noise in NDVI time-series. *International Journal of Remote Sensing.*, *13*, 1585–1590.

White, M. A., Thornton, P. E., & Running, S. W. (1997). A continental phenology model for monitoring vegetation responses to interannual climatic variability. *Global Biogeochemical Cycles*, *11*, 217–234.

White, M. A., Running, S. W., & Thornton, P. E. (1999). The impact of growing-season length variability on carbon assimilation and evapotranspiration over 88 years in the eastern US deciduous forest. *International Journal of Biometeorology*, *42*, 139–145.

White, M. A., Nemani, R. R., Thornton, P. E., & Running, S. W. (2002). Satellite evidence of phenological differences between urbanized and rural areas of the Eastern United States deciduous broadleaf forest. *Ecosystems*, *5*, 260–277.

Wolfe, D. W., Schwartz, M. D., Lakso, A. N., Otsuki, Y., Pool, R. M., & Shaulis, N. J. (2005). Climate change and shifts in spring phenology of three horticultural woody perennials in northeastern USA. *International Journal of Biometeorology*, *49*, 303–309.

Zhang, X., Friedl, M. A., Schaaf, C. B., Strahler, A. H., Hodges, J. C. F., Gao, F., et al. (2003). Monitoring vegetation phenology using MODIS. *Remote Sensing of Environment*, *84*, 471–475.

Zhang, X., Friedl, M. A., Schaaf, C. B., & Strahler, A. H. (2004a). Climate controls on vegetation phenological patterns in northern mid- and high latitudes inferred from MODIS data. *Global Change Biology*, *10*, 1133–1145.

Zhang, X., Friedl, M. A., Schaaf, C. B., Strahler, A. H., & Schneider, A. (2004b). The footprint of urban climates on vegetation phenology. *Geophysical Research Letters*, *31*, L12209.